NOVA SCHOOL OF SCIENCE & TECHNOLOGY

Departament of Materials Science

Ricardo Jorge Lima Cabral

BSc in Micro and Nanotechnology Engineering

Impedance Sensing Device for Wound Monitoring

MASTER IN MICRO AND NANOTECHNOLOGY ENGINEERING

NOVA University Lisbon
September, 2023

NOVA SCHOOL OF SCIENCE & TECHNOLOGY

Departament of Materials Science

Impedance Sensing Device for Wound Monitoring

Ricardo Jorge Lima Cabral

BSc in in Micro and Nanotechnology Engineering

Adviser: Prof.Dr. Rui Alberto Garção Barreira do Nascimento Igreja
Associated Professor, NOVA University Lisbon

Co-advisers: Master Tomás Pinto e Cruz de Oliveira Pinheiro
PhD Student, NOVA University Lisbon

Examination Committee:

Chair: Prof.Dr. Hugo Manuel Brito Águas,
Associated Professor, NOVA University Lisbon

Rapporteurs: Prof.Dr. Joana Maria Dória Vaz Pinto Morais Sarmento
Assistant Professor, NOVA University Lisbon

Adviser: Prof.Dr. Rui Alberto Garção Barreira do Nascimento Igreja
Associated Professor, NOVA University Lisbon

Members: Master Tomás Pinto e Cruz de Oliveira Pinheiro
PhD Student, NOVA University Lisbon

MASTER IN MICRO AND NANOTECHNOLOGY ENGINEERING

NOVA University Lisbon
September 2023

Impedance Sensing Device for Wound Monitoring

Copyright © Ricardo Jorge Lima Cabral NOVA School of Science and Technology, NOVA University Lisbon.

The NOVA School of Science and Technology and the NOVA University Lisbon have the right, perpetual and without geographical boundaries, to file and publish this dissertation through printed copies reproduced on paper or on digital form, or by any other means known or that may be invented, and to disseminate through scientific repositories and admit its copying and distribution for non-commercial, educational or research purposes, as long as credit is given to the author and editor.

This document was created with Microsoft Word text processor and the NOVAthesis Word template [1].

ACKNOWLEDGMENTS

First of all, I would like to thank my supervisor Professor Rui Igreja, my co-supervisor Tomás Pinheiro and the entire team at laboratory two for giving me all the tools to make this work possible. It has been a long season but thank you for all your help and the tools I needed to get to the end.

To my family, for being so far away, but so near at the same time, thank you for giving me all the support I needed, even though I only came home a few times, you were always by my side on this long road and for always being patient with me and believing in me. Without you, nothing would have been possible and all it is journey has been made possible by the tireless support I've always had from you, thank you.

To my lifelong friends, Maria Inês and Pedro, thank you for always being there for me, for always caring and never saying no to a request for help.

To my friends during these five years, Barbara Sieira, Manuel Macedo, Mariana Baptista, Barbara Carmo, André Pequito, Guilherme Correia and Daniel Rodrigues for the support they gave me, for the late nights studying, for the dinners and even though they were far away during the final stage, they were always there and always ready to lend a hand, thank you for everything.

To AEFCT, especially to my Administrative Area, for the great support you gave this year, which I can say was the best year of these 5 years thanks to you, I know it wasn't easy, but you were always there for me, thank you for the words, the affection, the many lunches, for above all being there for everything. Thank you to the best team AEFCT has ever had, we are giants, and nothing stops us. To Sónia Pereira, a second mum, who even without me saying anything knows how to solve everything and always pull me up, thank you for everything. I couldn't finish this acknowledgement without telling Vasco Amaral thank you for always being just a phone call away, for being my right-arm this past year and for always supporting me, even when it seemed impossible, you were there, you're a machine, thank you.

To Silvia Duarte, even away from the sport that unites us, always concerned and always ready to help with anything, thank you for always believing in me.

Finally, to my biggest headache Catarina Patrão who, above all else, was a great support this year and all the tireless support you give me, without whom none of this would be possible, thank you.

“Life is like riding a bicycle. To keep your balance, you must keep moving.”
(Albert Einstein).

ABSTRACT

A wound develops when a specific area of the body is exposed to prolonged pressure/cutting. In order to analyze the condition of the wound, it is necessary to take into account various parameters such as pH and humidity.

The research work presented in this dissertation focuses on the study and optimization of an impedance device for measuring wound status. To fabricate this device, the laser irradiation technique was used, which consists of Laser Induced Graphene (LIG), a highly attractive material for creating and standardizing graphitic structures and electrodes specifically designed for use in electrochemical biosensors. Electrochemical Impedance Spectroscopy (EIS) was use to analyse the pH and humidity, providing a concise analysis of the control values for future application to the wound.

During this project, efforts were made to develop a device capable of measuring variations in pH and humidity, so it was necessary to construct an electrode array capable of measuring all these variations. After analysing the device, Raman peaks were identified with I_{2D}/I_G and I_D/I_G peak ratios of 0.59 and 1.18, respectively, showing low defect densities of LIG chemical structures and sheet resistances as low as 30.01 $\Omega.\,\mathrm{sq}^{-1}$.

After ensuring that the entire graphitisation process had been carried out successfully, impedance measurements were taken at pHs 3.5, 4.5, 6, 7.5 and 8.5, as well as humidity measurements over time, which allowed us to identify alterations around the electrodes and in view of these alterations could be suitable for future use on wounds.

Keywords: Wound Skin, Electrochemical Impedance Spectroscopy, Laser Induced Graphene

RESUMO

Uma lesão desenvolve-se quando uma área específica do corpo é exposta a uma pressão prolongada/corte. De forma a analisar o estado da ferida é necessário ter em conta diversos parametros como o pH e humidade.

A presente tese foca-se no estudo e optimização de um dispositivo de impedância para medir o estado da ferida. Para a produção desse dispositivo foi utilizado a técnica de irradiação laser, que consiste em Grafeno Induzido por Laser (LIG), um material altamente atrativo para a criação e uniformização de estruturas e elétrodos de natureza grafítica, sendo especialmente projetados para uso em biossensores eletroquímicos. Para análise do pH e da humidade foi utilizada a técnica de Espectroscopia de Impedância Eletroquímica (EIS) que permite uma análise concisa dos valores de controlo para uma futura aplicação na ferida.

Com decorrer deste projeto, foram feitos esforços para desenvolver um dispositivo capaz de medir variações de pH e de humidade.Posto isto, foi necessário construir uma matriz de elétrodos capaz de medir todas estas variações. Após análise do dispositivo, foram identificados picos Raman, com rácios de picos I_{2D}/I_G e I_D/I_G de 0,59 e 1,18 , respetivamente, apresentando baixas densidades de defeitos de estruturas químicas de LIG e exibindo resistências de folha tão baixas como 30 $\Omega.\,\mathrm{sq}^{-1}$.

Após a garantia que todo o processo de grafitização decorreu com sucesso, foram efetuadas medições de impedância entre os valores de pH 3.5, 4.5, 6, 7.5 e 8.5 e de humidade ao longo do tempo, que nos permitiu indentificar alterações ao redor dos eletrodos e face a estas alterações poderá ser apropriadao para no futuro usar nas feridas.

Palavras chave: Ferida Cutânea, Espectroscopia de impedância eletroquímica, Grafeno Induzido por Laser

CONTENTS

LIST OF FIGURES

LIST OF TABLES

ACRONYMS

PET	polyethylene terephthalate
PI	polyimide
LIG	laser-induced graphene
EIS	electrochemical impedance spectroscopy
DC	direct current
ZIF	zero insertion force
PPI	points per inch
BR	britton–robinson buffer method
SEM	scanning electron microscopy
EDX	energy dispersive x-ray spectroscopy

SYMBOLS

A	cross-sectional area
C_{dl}	double layer capacitance
I	current
I_{2D}	intensity of Peak 2D in Raman spectroscopy
I_D	intensity of Peak D in Raman spectroscopy
I_G	intensity of Peak G in Raman spectroscopy
L	length
pH	hydrogen potential
R	electrical resistance
R_{ct}	charge transfer resistance
R_u	ionic resistance
R_S	sheet resistance
V	voltage
W	width
Z	magnitude of impedance, ohm
Z_W	warburg impedance
Z'	real part of the impedance
Z''	imaginary part of the impedance
$	dollar
ΔZ	variation in magnitude of impedance
θ	phase shift
ρ	material resistivity

1

INTRODUCTION

1.1 Impact on the population

As chronic skin lesions have been dubbed the "hidden pandemic" and are a danger to both the economy and public health, the demand for a more efficient treatment has become more apparent. The annual cost of treating chronic wounds is estimated at $25 billion, with $11 billion alone being towards treating individuals that suffer from pressure ulcers, a chronic lesion with a particularly high incidence of morbidity that affects over 2.5 million people in the United States. The prediction is for the continuous aggravation of the problem, as these skin wounds are more frequent in diabetic, obese or elderly people, and there has been a both fast global rise in obesity, diabetes and the aging of the population of the United States.[1]

When it comes to the wound healing process, it is closely regulated by cytokines and involves distinct phases of inflammation, tissue growth and tissue remodelling.This process relies on several essential factors in relation to the state of the wound, including pH and humidity.[2] Monitoring the pH level is vital to understanding the state of the wound. In the normal state of the skin, there is an acidic environment with pH values between 4 and 6, first explained by Hesus et al. in 1892[3] and later by Schade and Marchionini in 1928 [4]. This value varies according to the anatomical location and age of the person. Moisture has an important role to play in wound monitoring, as it provides valuable information about the state of the wound. It is important to note that there is no universally accepted specific moisture percentage value for all wounds, as moisture requirements can vary depending on the type and severity of the injury, as well as the individual conditions of the patient.[5][6]

1.2 Literature review

Various devices are currently being developed to treat and assess the condition of wounds, such as electronic devices that use impedance spectroscopy to non-invasively map tissue damage, as impedance is highly correlated with tissue health in a variety of animals and wound types. [1]

Among these electronic devices, there is the one developed by A. Kekon et al. . The Figure 1 which consists of a set of electrodes printed on a sheet of polyethylene terephthalate (PET), on which the biomedical grade carbon ink electrodes are manufactured using the screen printed technique. [7]. The device depicted on Figure 2 was developed by M.J. Chaudon and the electrodes are made up of three different layers that are screen printed on flexible plastic substrates made from PET. [8].

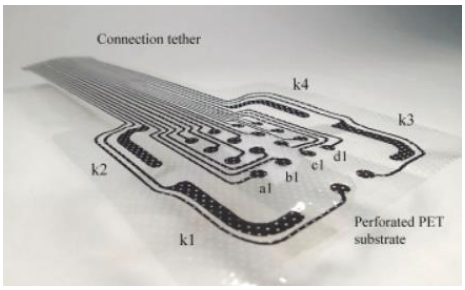

Figure 1 - Sensor example developed by A. Kekonen et al. [7].

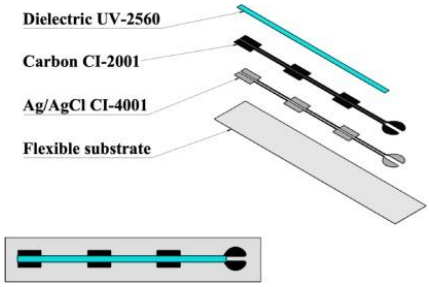

Figure 2 - Sensor example developed by by M.-J. Chaudon [8].

As is mentioned above, both projects use PET as a substrate, but one of the major disadvantages of this is that it is made from petroleum, a non-renewable source, and, when mixed with other types of materials, it becomes unviable for recycling. However, in all our work we will use paper as the first substrate and then polyurethane. Paper is a natural resource that is easy to access and dispose of, as well as being easily recyclable. Polyurethane, which has a fairly simple production process based on the reaction between diisocyanate and polyester diol, also has excellent properties, namely good resistance to adhesion, high chemical resistivity, excellent drying and flexibility, which make polyurethane one of the most suitable polymers for this use. [9] [10]

In terms of the techniques used, both systems use screen printing to produce the sensor, which has many drawbacks, such as the use of masks, the curing time required, the difficulty of changing the patterns during the optimisation process and the viscosity of the ink, which affects the electrochemical properties of the system itself. Throughout our project, we will be using the laser irradiation technique, which doesn't require a mask and is a versatile, fast, high performance prototyping technique with easy pattern change, making it the most fitting technique for this application.[11]

Regarding the measurement technique, both projects use the Electrochemical Impedance Spectroscopy technique, which, due to its many advantages, was considered to be the most appropriate.

With these considerations in mind, we will now explain the techniques mentioned above.

1.3 Laser Irradiation

To manufacture the electrodes, Laser Irradiation will be used, which requires the usage of graphene. Graphene is a two-dimensional carbon structure composed of a hexagonal arrangement of carbon atoms that exhibits unusual physical (namely electrical, thermal, mechanical, and optical) and chemical properties, primarily due to its exceptionally high electron mobility, thermal conductivity, and mechanical strength. [12]

The resulting laser-induced graphene (LIG) exhibits high electrical and thermal conductivity, and can be readily patterned for interdigitated electrodes for micro supercapacitors and sensory devices.[13], [14]

The use of laser induced graphene has several advantages, such as projectable standardisation, environmental compatibility, adjustable compositions, controllable morphologies, good resolution, and processing speed. In addition to these, LIGs have high porosity, great flexibility, and mechanical robustness. [15]

1.4 Electrochemical Impedance Spectroscopy

The electrochemical impedance spectroscopy (EIS) is based on the application of a small amplitude stimulus (voltage or current), usually superimposed on a DC signal (voltage or current), to an electrochemical system and the measurement of the resulting response (current or voltage) over a wide frequency range. That said, it is essential that measurements are carried out by applying a small amplitude disturbance to guarantee a linear relationship between the applied signal and the system's response. One of the great advantages of this technique is that it simulates the data for an equivalent electrical circuit and thus retrieves numerical values for the components included in the circuit,Figure 3.[16]

For sensor applications, impedance data is usually presented in a complex plane graph, where the real part (Z') is represented on the x-axis and the imaginary part (Z'') on the y-axis, which is also referred to as a "Nyquist plot". The benefit of this representation is that the characteristics of the impedance spectrum at lower frequencies are more prominent than those at higher frequencies (often the lower frequency phenomena are the most important in sensors), while the downside is that the frequency values are not explicitly shown. An alternative representation is the Bode representation, which shows the magnitude of the impedance and phase angle as a function of the logarithm of the frequency, which shows all the information but is not as easy to visualise the physical model of the system at low frequency.[17]

However, in real electrochemical systems, the Nyquist plot described in Figure 3 is expected for a faradaic impedance spectrum over a wide frequency range usually includes both the semicircle (in this frequency range, the electrochemical process is controlled by charge transfer phenomena) and the straight line (in this frequency range, the electrochemical process is controlled by mass transfer phenomena), parts which may differ depending on the respective values that consists of an active electrolyte resistance R_u in series with the parallel combination of the double-layer capacitance C_{dl} and an Warburg impedance Z_W of a faradaic reaction in series with charge transfer resistance R_{ct}. [16]

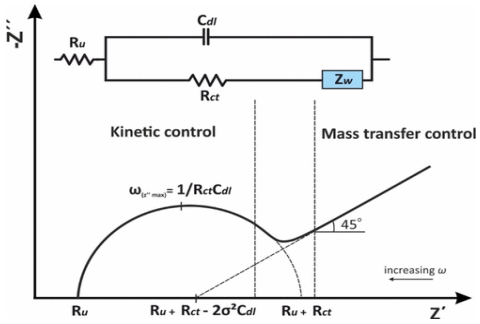

Figure 3 -Randles' equivalent electrical circuit over a wide frequency range

2

MATERIALS AND METHODS

This section first describes the process used to fabricate the sensors on all substrates. This is followed by the parameters used in the VLS3.50 CO_2 laser system, the characterization carried out to measure the response of the sensors, and finally the protocol used to collect and analyze the data.

2.1 Sensor manufacturing

Before the manufacture of the sensor, Whatman Grade 1 chromatography paper (Whatman International Ltd, Florham Park, NJ, USA) had to be chemically prepared. To do this, the paper was first cut to A6 format (105-148 mm) and, after 20 minutes in a solution of sodium tetraborate decahydrate(0.1 M), for each side, the sheets were dried overnight in an oven at 50°C. The utilization of sodium tetraborate decahydrate allowed water to be released from the paper substrate, thus helping as a fire retardant. This is a crucial step for laser irradiation, as it improves the substrate's resistance to the heat generated by the laser by acting as a chemical heat sink, thus reducing thermal degradation.

The next step was to designsensor the system, based on the sensor by A. Kekon et al. , using vector image software (Adobe Illustrator, Adobe Systems software, Ireland) and then a computer controlled CO_2 laser cutting machine (VLS 3.50, Universal Laser Systems) was used to engrave it onto the pre-treated paper substrate, pictured on Figure 4. Each electrode has a dimension of 2 mm, and this distribution was used so that different wound sizes could be measured. It was subsequently transferred to a $12 \times 6\ cm$ adhesive (BSN Medical, Fixomull Transparent) using a water transfer process developed by T. Pinheiro et al. in 2022, Figure 4 B.[18] Subsequently, the adhesive was covered with adhesive tape to act as a mask for the contact painting process, so that the conductive tracks could be created using conductive silver ink (AG-510 silver ink, Conductive Compounds, Inc., Hudson) over the corresponding openings in the passivation layer. After curing on a hot plate (50ºC, 1 h), the adhesive masks were removed, Figure 4 C. Silver paint was then applied to the polyimide (PI) in the LIG area corresponding to the connections of the ZIF plugs. Finally, the sensors were covered with adhesive tape, which had an opening in the area where the measurement sensors were located, Figure 4 D, and then connected to the ZIF plugs, ready to be tested, Figure 4 E, concluding the fabrication process for the system.

(A) (B) (C)

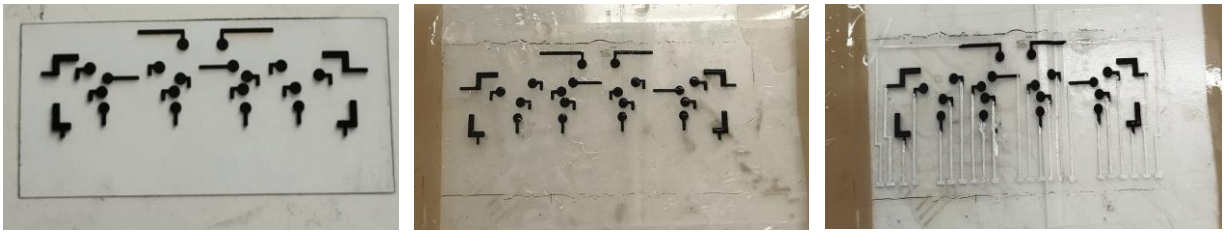

(D) (E)

Figure 4 - Manufacturing processes. (A) Recording of the circuit on the pre treated paper substrate. (B) Water transfer process. (C) Painting process of the conductive tracks. (D) Location of measurement sensors. (E) Connection to ZIF plugs.

2.2 Laser Property and LIG Characterization

A VLS3.50 CO2 laser system from Universal Laser Systems was used to make the treated paper substrates. With a maximum output of 50 W and a maximum scan speed of 127 cm/s, this laser system can produce a pulsed beam with a wavelength of 10.6 m photons. This method enables the selection of points per inch (PPI) up to a maximum of 1000 PPI (393 points per cm) for the modification of pulse density. As such, for different raster speed settings, the laser pulses operate at distinct frequencies. [19]

Constant power and speed percentage settings were used in every film engraving for all the studied irradiation planes, more specifically 5% power, 5% speed and 1000 PPI, as mentioned by Coelho, J et al in 2023. [20]

2.3 LIG Characterization

The previously formed LIG was characterised by SEM (Hitachi TM 3030Plus Tabletop) to obtain a visual image of the LIG 3D networks. The chemical composition of the LIG on the paper substrates was also studied by SEM using EDX to provide a visual inspection of the distribution of elements in the samples.The electrical resistance of the sheet (Rsh, $\Omega.sq^{-1}$) was determined by voltammetry measurements in order to obtain obtain I/V plots, with the aid of a PalmSens 4.0 potentiostat (PalmSens Compact Electrochemical Interfaces), and from these to derive the desired values. Raman measurements were performed using a Renishaw inVia Qontor (Gloucestershire, UK) confocal Raman microscope equipped with a Renishaw Centrus 2957T3 detector. The laser beam was focused through a $50\times$ Olympus objective and measurements were performed using the 633 nm laser. Three measurements were taken on each sample in predetermined areas of the location covered by the LIG.

2.4 Measurement protocol

2.4.1 Electrolyte preparation

To begin the measurement process, solutions at pHs 3.5, 4.5, 6, 7.5 and 8.5 were needed, so the Britton-Robinson (BR) buffers method was followed. Starting with a 100 ml solution of Milli-Qultrapure water of laboratory quality and mixing 0.238 ml of phosphoric acid - H_3PO_4, 0.238 ml of acetic acid - CH_3COOH and 0.2473 g of boric acid - H_3BO_3 (the first purchased from Panreac AppliChem and the rest from Sigma-Aldrich). After finalizing this solution, the dilution process was employed in order to obtain the solutions with the desired pHs. Thereafter, the collection of results will begin.

2.4.2 Electrochemical characterization

The sensors were subjected to electrochemical characterization to determine the experimental parameters. Electrochemical measurements were carried out using a PalmSens 4.0 potentiostat and the EIS was conducted with a pulse of 1 mV amplitude, 250 data points, in a frequency range of 1000 to 1 Hz. For this measurement, 10 µl were inserted between the two electrodes of the sensor and then the measurements were taken from the connection to the ZIF Plug.

3

RESULTS AND DISCUSSION

This section first describes the process used to fabricate the sensors on all substrates. This is followed by the parameters used in the VLS3.50 CO_2 laser system, the characterization carried out to measure the response of the sensors, and finally the protocol used to collect and analyze the data.

3.1 Manufacturing Steps

In a first approach, our circuit consisted mostly of graphene from the laser, Figure 5 A, but several problems arose during the transfer process to the adhesive. As a result, it was necessary to reduce the amount of graphene to allow a successful transfer, Figure 5 B, after which the rest of the conductive tracks were created using silver conductive ink, thus achieving the initially intended result,Figure 5 C.

(A) (B) (C)

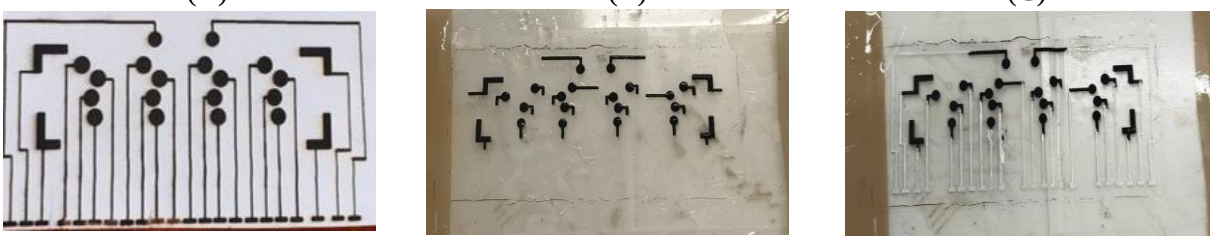

Figure 5 - Manufacturing Steps. (A) Use of graphene throughout the circuit. (B) Graphene reduction for successful transfer process. (C) Completion of the initially idealized circuit

3.2 Paper-based LIG characterization

A detailed physico-chemical characterisation of the LIG after the transfer and the LIG on the paper substrate was conducted in order to obtain information on its chemical, electrical and morphological properties.

The morphological study of the paper based LIG produced and transferred was performed by SEM to understand the effect of the different states on the surface of the carbon fibres.

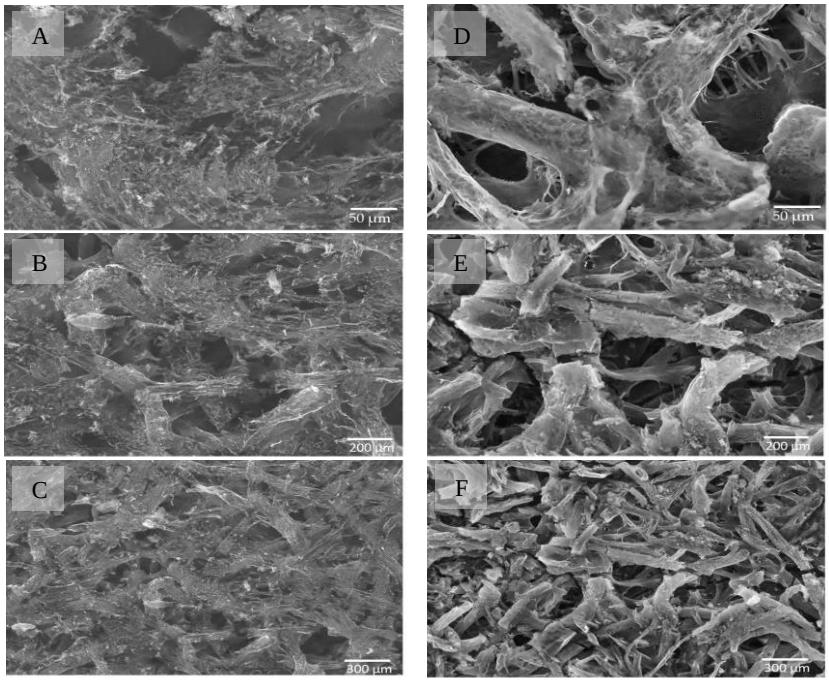

Figure 6 - Scanning electron microscopy study of the surface morphology of paper with LIG (A, B and C) and LIG after transfer (D, E and F)

Analysis of both types of process revealed different architectures of the fibres involved. In morphological terms, the paper is made up of compacted cellulose fibres resulting in a random distribution of pores. When the laser is applied to the paper, there is a degradation of the fibres, where part of these fibres as well as the carbon fibres can be identified in Figure 6 B. After transfer, the opposite surface of the LIG is exposed. This surface, due to its greater depth during laser irradiation, is not as subject to high laser temperatures, resulting in less pronounced degradation. This preserves the original morphology of the paper fibres in the carbonised material, Figure 6 E.

After collecting these images, the analysis of the chemical composition of the LIG on the paper substrates is made, using EDX by SEM to provide a visual inspection of the distribution of the elements in the samples.

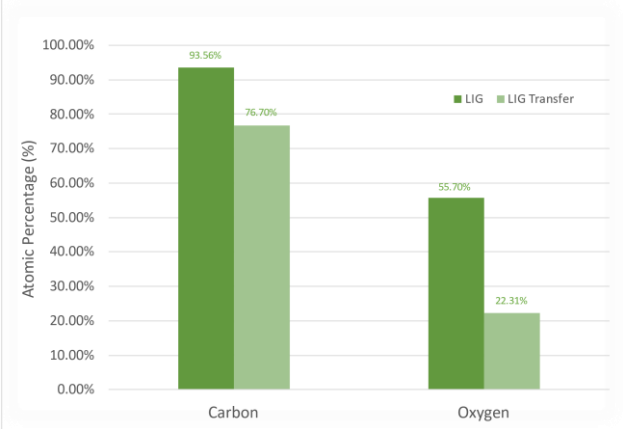

Figure 7 - Measurements by EDX

After laser irradiation, an increase in the carbon content of the LIG sample was observed, along with a simultaneous decrease in the oxygen content, as shown in Figure 7. Initially, a high carbon concentration was present due to the predominance of graphene for the graphitisation process on the paper substrate. However, with the subsequent transfer, there is a loss of graphene, which can be explained by the decrease in the amount of carbon. However, with the subsequent transfer, the part that we see is the one that has not been exposed to such high temperatures on the surface directly exposed to the laser, there is a decrease in the percentage of carbon.

The chemical structure of LIG produced under optimised conditions was studied by Raman spectroscopy (Figure 8).

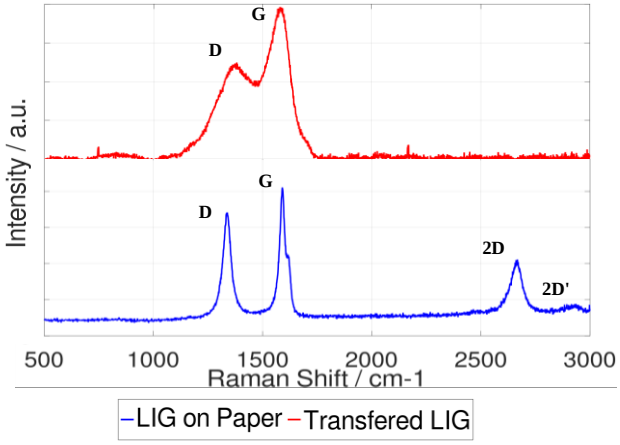

Figure 8 - LIG Raman spectra of paper with LIG and LIG after transfer.

In the LIG, three signature peaks are found at around 1338 cm^{-1}, 1587 cm^{-1} and 2672 cm^{-1}, corresponding to the D, G and 2D peaks characteristic of carbon based structures. The D peak is generally associated with the degree of defects in the sample, the G peak is produced by graphitic carbon and the 2D peak is associated with photons from the second order zone boundary. Since the D peak is attributed to sp2 carbon hybridisation defects in hexagonal sheets of carbon atoms, the presence of this peak indicates a defective graphene structure due to distorted sp2 carbon networks. The G peak results from first order inelastic processes attributed to bond stretching of sp2 atoms in the graphite structure. The peak that showed the strongest dependence on the laser and paper substrate parameters was the 2D peak, attributed to the second order two photon resonance process. The 2D graphite peak consists of two peaks (2D and 2D') usually observed at 2725 cm^{-1}. In addition, since the intensity ratio $I_{2D} / I_G < 1$ and $I_G/I_D > 1$, it is assumed that the obtained samples consist of folded graphene sheets with few layers and a smaller defect, which shows that the graphitisation process was successful. [21]–[25]

In the transferred LIG, only 2 signature peaks were observed at around 1370 $cm^{-1}$and 1580 cm^{-1}, corresponding to the D and G peaks, which, after the transfer of the LIG structures, the surface of the pattern is exposed to the laser, leading to a very different Raman profile. This exposure leads to the visualization of graphene oxide, represented by the absence of the 2D peak and the increased width of the G and D peaks. [18]

As for the electrical study, it was executed by measuring the resistance value of a 2 cm LIG line. To obtain these values, 4 tests were performed on each sample and then the resistivity was calculated from the I/V curves, as described in Figure 9.

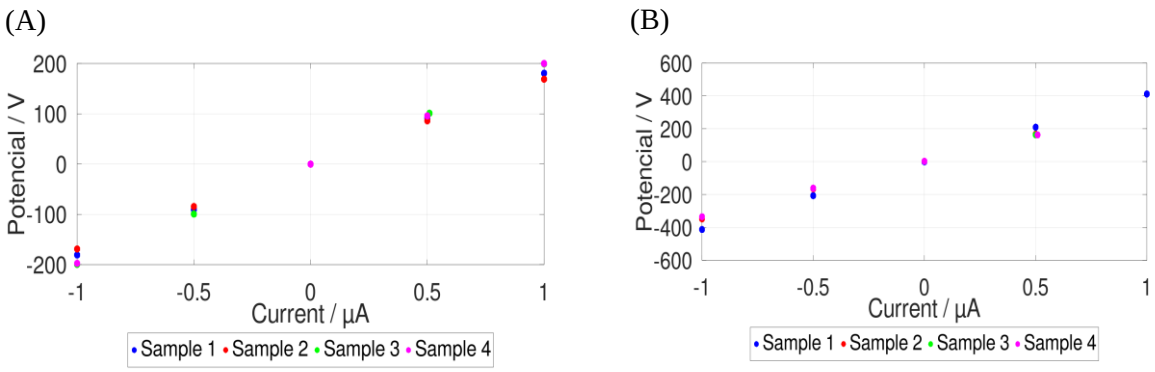

Figure 9 - I/V curves with 4 collections. (A) Paper with LIG. (B) LIG after transfer.

Table 1 - Resistance values for the two samples obtained by linear fitting.

Paper with LIG	**LIG after transfer**
Resistance Value	Resistance Value
$\boldsymbol{R = 5,41 \pm 0,51\ K\Omega}$	$R = 3{,}01 \pm 0{,}58$ KΩ

The resistance value was obtained by calculating the average of the 4 samples and then measuring the thickness of the LIG,

Table 1. To do this, several thickness measurements were taken in order to find a uniform thickness value, 0.56 µm, measured by a micrometer between the zone without graphene and with graphene. After this, the values of the resistivity, conductivity and sheet resistance were reached, Table 2, formulas in A.1.1.

Table 2 - Calculation of the resistivity, conductivity and sheet resistance

	Resistivity	**Conductivity**	**Sheet Resistance**
Paper with LIG	$\rho = 0{,}003\ \Omega/\mathrm{m}$	$\sigma = 3{,}3\ \mathrm{S/cm}$	$R_s = 54{,}1\ \Omega/\mathrm{sq}$
LIG after transfer	$\rho = 0{,}002\ \Omega/\mathrm{m}$	$\sigma = 5{,}9\ \mathrm{S/cm}$	$R_s = 30{,}1\ \mathrm{S/sq}$

After the transfer, there is a visible increase in the strength properties, which can be explained by the fact that the transfer process leads to an upturn in the amount of amorphous carbon on the surface. The opposite is observed for conductivity, which could be due to the decrease in the amount of carbon in the sample.

3.3 Measurement parameters in a sensor

To test the sensor, all points along it were measured, while keeping all conditions constant in a pH 6 solution. For these measurements, we used the following configuration to know the position of each sensor we were measuring, Figure 10. This orientation was as a guide used so that we could identify the electrode pairs between measurements.

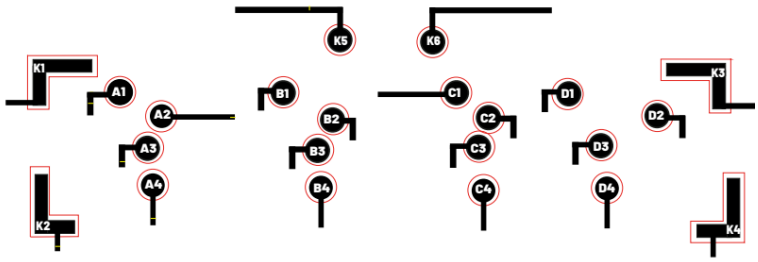

Figure 10 - Circuit with ordering for measurements.

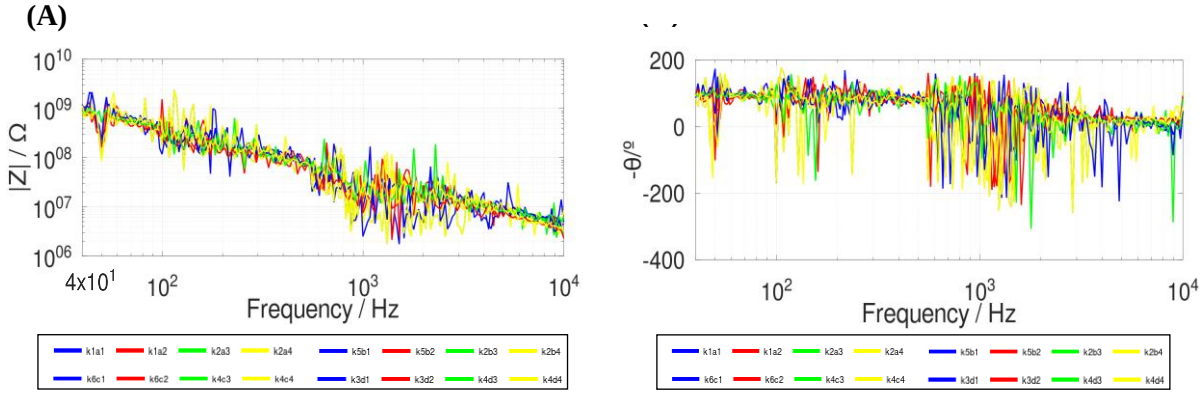

Figure 11 - Measurement at all points on the sensor by potentiostat, (a)

Analysing Figure 11, it is apparent that, at all points, the initial and final impedance values remained practically constant, proving that the sensor is uniform throughout. This noise could be due to unstable contact between the plug and the sensor or between the plug and the device.

3.3.1 pH variation measurement

3.3.2 Parameters

3.3.2.1 Introduction

In the skin's normal state, an acidic environment is recorded with pH values between 4 and 6, first explained by Hesus et al. in 1892 [3] and later by Schade and Marchionini in 1928 [4]. This value varies according to the anatomical location and age of the person.

In the presence of a wound, this acidic environment is compromised, resulting in the infected area to register a pH between 7 and 8.5. This stems from the fact that the exposed tissue has a pH more similar to the one of the inside of the body and due to the presence of different types of enzymes and

human pathogenic bacteria, which cause its increase. At a pH below 6 their development is inhibited.[26][27]

For this parameter, we made 3 different measurements with t_1=5 minutes, t_2=10 minutes, and t_3 = 15 minutes.

3.3.2.2 Bode Diagrams

3.3.2.2.1 Measurements on pairs of electrodes, A1 and A3, 10 mm apart

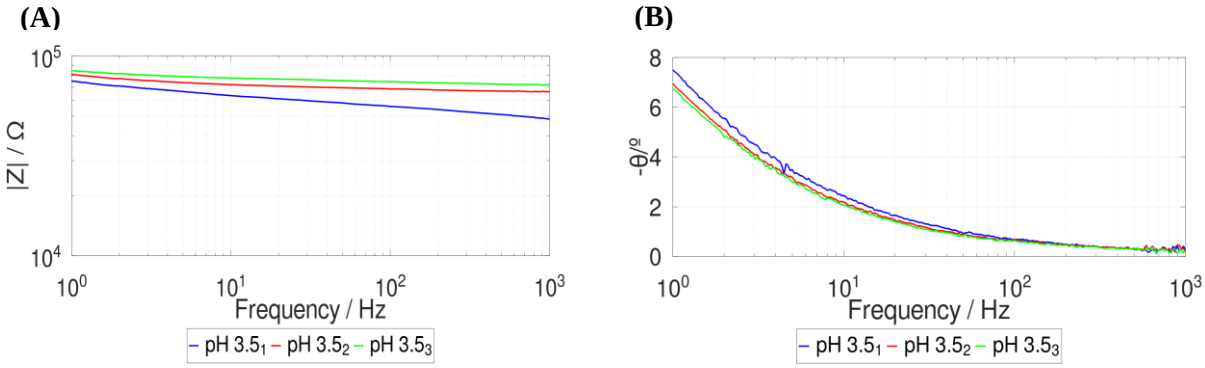

Figure 12 - Bode Diagrams at a pH of 3.5 in pairs of electrodes 10 mm apart. (A) Impedance by Frequency. (B) Phase by Frequency.

For 10 mm, it can be seen that, at low pH values, there is a greater oscillation in the impedance values at low frequencies compared to high pH values. Furthermore, the impedance value remains practically the same at low and high frequencies, which shows that the system is stable and has little noise. As for the phase, this oscillation is practically constant throughout the measurements, with only the high frequencies showing noise, which could be due to an initial connection problem. Figures with other pH values shown in A.2.1.

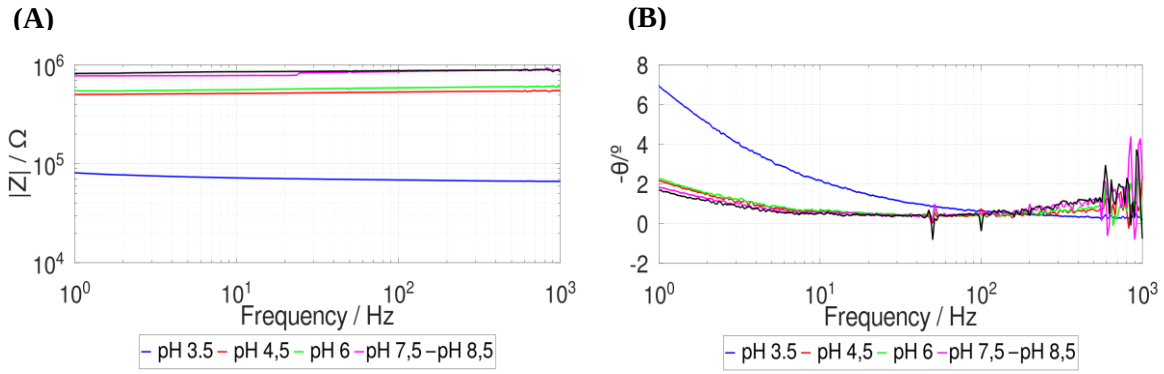

Figure 13 - Bode Diagrams at all pHs in pairs of electrodes 10 mm apart. (A) Impedance by Frequency. (B) Phase by Frequency.

In this graph, the measurement of t is fixed at 10 minutes for all pH values and, as expected, between an impedance value of 9×10^4 Ω and 6×10^5 Ω, the skin has a pH between 3.5 and 6, which indicates that, at this impedance, the skin tissue is healthy. At a higher impedance than the aforementioned one, i.e. approximately 8×10^5 Ω, the pH value is greater than 6, which indicates that the tissue is infected. Furthermore, from this analysis, when the skin's impedance is greater than 6×10^5 Ω, we are in the presence of a wound. The increase in the impedance value from pH 3.5 to 8.5 is due to the resistance of the solution contributing to the impedance of the sensor, and is mainly caused by the higher resistance of the alkaline solutions applied compared to the acidic solutions.[28]

3.3.2.2.2 Measurements on pairs of electrodes, A1 and A2, 3 mm apart

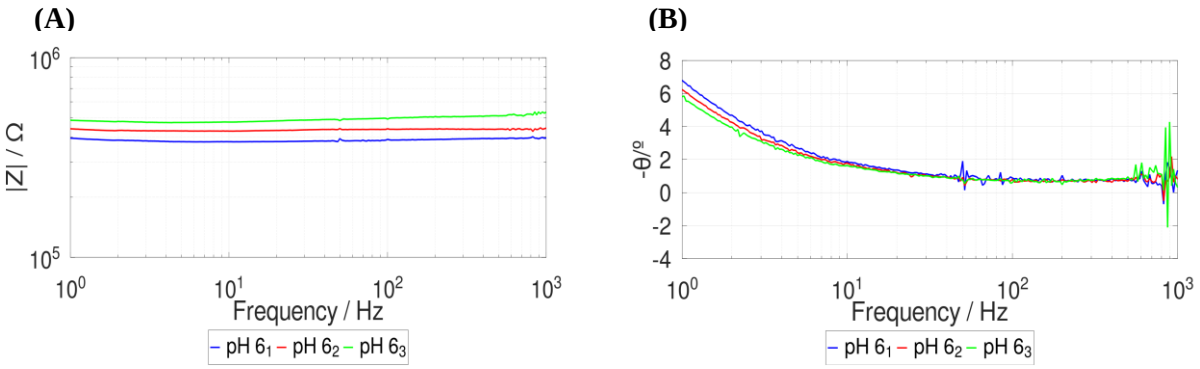

Figure 14 - Bode Diagrams at a pH of 6 in pairs of electrodes 3 mm apart. (A) Impedance by Frequency. (B) Phase by Frequency.

At 3 mm, the difference in impedance between the 3 measurements is minimal and there is little noise, which shows that the system is stable and that with closer pairs of electrodes we can obtain more uniform values over time. However, as far as the phase is concerned, noise is observed, which can be caused by the proximity of the pair of electrodes, which can short-circuit during the measurements, something that should be minimised and controlled in this parameter. Figures with other pH values shown in A.2.2.

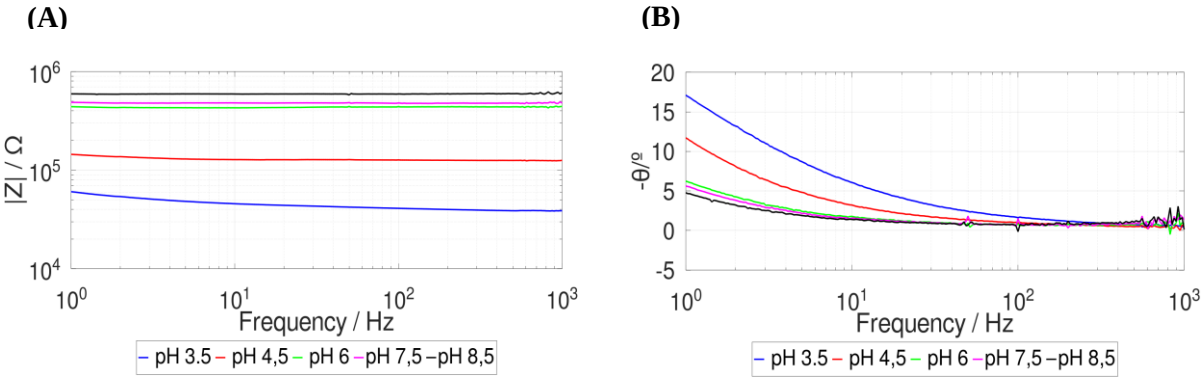

Figure 15 - Bode Diagrams at all pHs in pairs of electrodes 3 mm apart. (A) Impedance by Frequency. (B) Phase by Frequency.

At this distance, from a certain impedance value, $3 \times 10^6\ \Omega$, there is an acidic pH, so from this impedance value, it is guaranteed that the area in question is infected and this increase in impedance between the different pHs once again demonstrates that the resistance of the solution contributes to the impedance of the sensor.

Let's now analyse the frequencies to see the real difference pHs by impedance between the different frequency values.

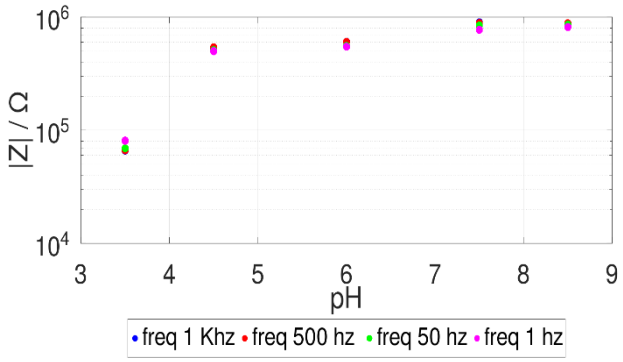

Figure 16 - Graph with the different pHs by impedance between the different frequency values

As Figure 16 shows, there is no significant difference in the pH values between the data collected, so a frequency of 50 Hz we be set to measure the difference more accurately.

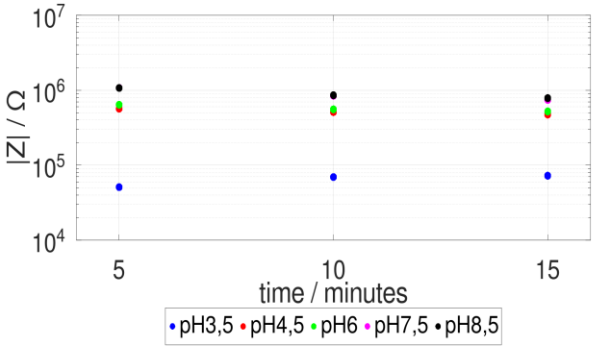

Figure 17 - Graph with the different pHs at a constant frequency over time.

Figure 17 refers to 3 measurements made of the pH level, where t=5 minutes corresponds to the first measurement, and t=15 minutes the last. Visualising it, there is a big difference in the impedance values between pH 3.5 and 4.5, which will be analysed in the following figure.

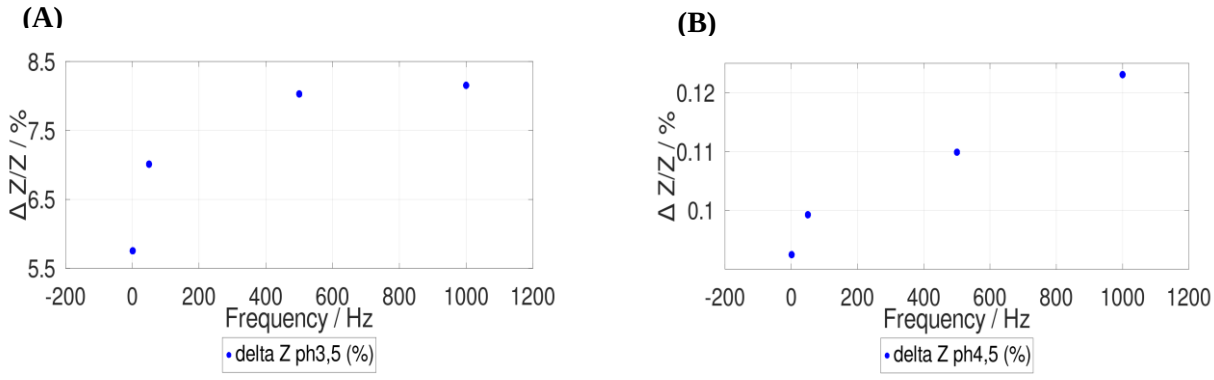

Figure 18 - Graph of Δ Z/Z percentage by frequency. (A) with pH 3.5. (B) with pH 4.5.

According to Figure 18, there is a large percentage discrepancy between the Δ Z of 4.5 and the Δ Z of 3.5, which may be caused by the high alkaline value of the electrolyte and the difference in pHs of less than 3 measurement units, whereas in other electrolyte solutions there is not such a large difference. Δ Z was calculated using the formula in A.1.2

3.3.2.2.3 Differences between Distance on pairs of electrodes, A1, A2 and A3

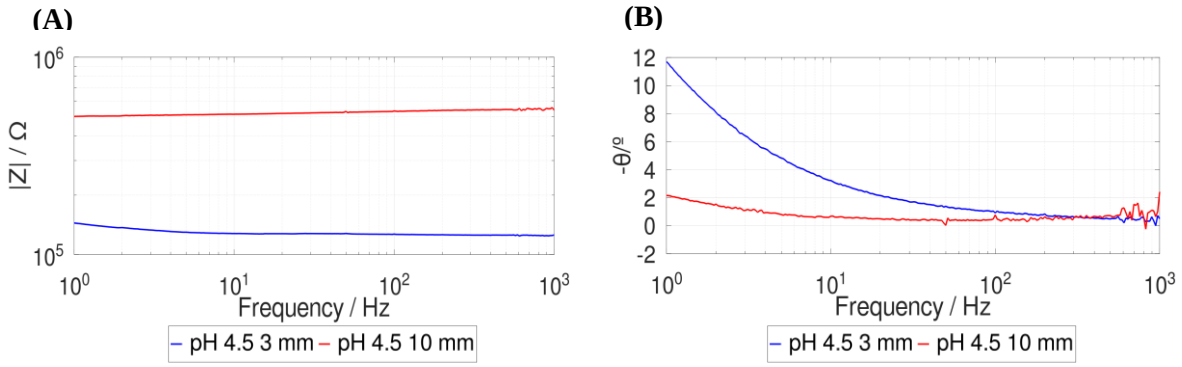

Figure 19 - Bode Diagrams at a pH of 4,5 in pairs of electrodes 3 mm and 10 mm apart. (A) Impedance by Frequency. (B) Phase by Frequency.

In these graphs,Figure 19 , time is fixed at 10 minutes for all pH values, and it can be concluded that the current distribution is variable with distance. However, it can be said that the greater the distance between the pair of electrodes, the greater the impedance value and, as far as the phase is concerned, that the closer the distance, the higher the value. Figures with other pH values shown in A.2.3.[29]

3.3.2.2.4 Measurements on pairs of electrodes, A1, A2 and A3, 10 mm and 3 mm apart

Throughout this subchapter, the graphs needed to first construct the Nyquist plot and then compare the measured values with the values obtained by the Randles Circuit will be presented.

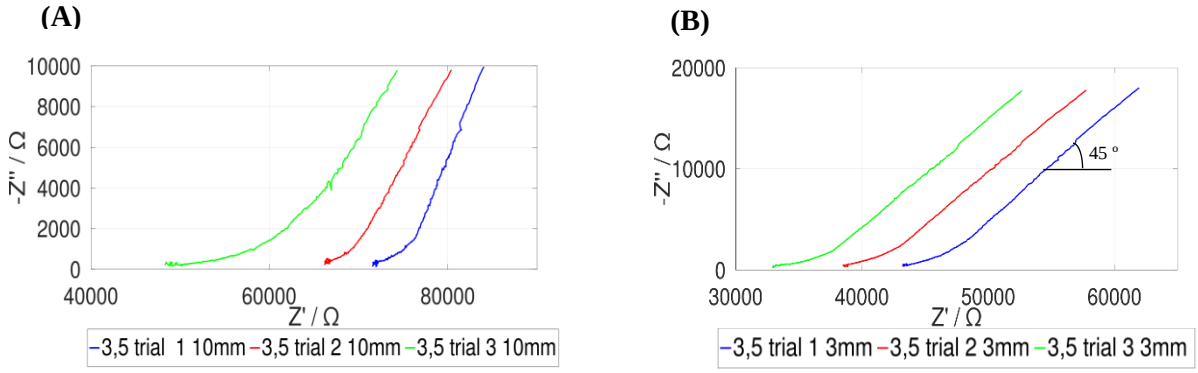

Figure 20 - Nyquist plot, at a pH 3.5, (A) 10 mm. (A) 3 mm.

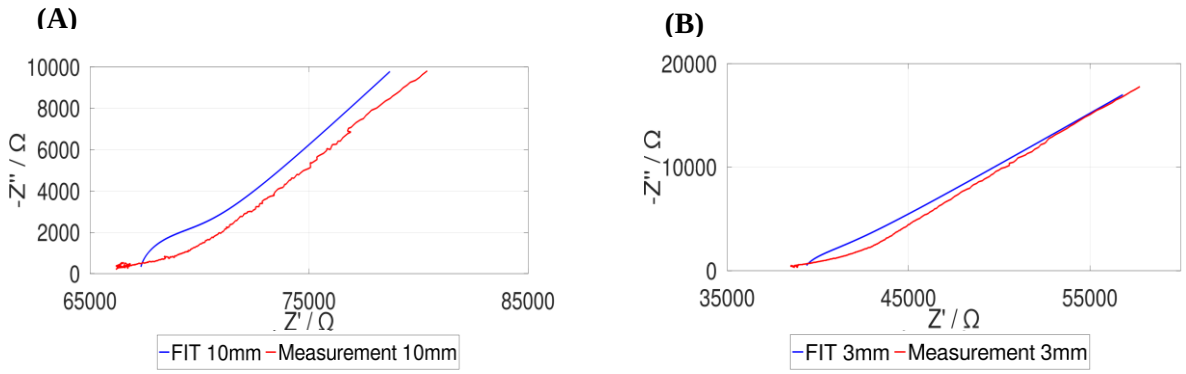

Figure 21 - Randles Circuit, at trial 2 at pH 3.5, (A) 10 mm. (A) 3 mm.

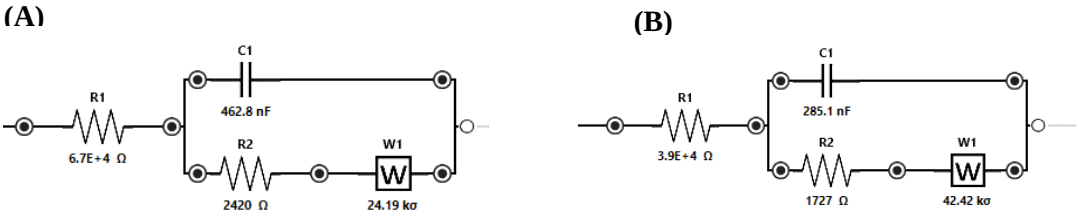

Figure 22 - Randles Circuit at a pH 3.5. (A) at 10 mm. (B) at 3 mm.

Table 3 - Evolution of the resistance value over time

	Randles circuit for 10 mm	**Randles circuit for 3 mm**
Time	Resistance	Resistance
5 minutes	7,2 MΩ	4,3 MΩ
10 minutes	6,6 MΩ	3,9 MΩ
15 minutes	4,8 MΩ	3,3 MΩ

By analysing the graphs, Figure 20 and Figure 21, we can confirm that we are in the Warburg impedance zone and, by Table 3, that the resistance value has been decreasing over time.. Visualising the Randles circuit, Figure 3, we can see that the value of the Warburg impedance is very high, which shows that, in this circuit, Figure 22, this impedance is dominant at all frequencies. [30]

3.3.3 Humidity measurements

3.3.3.1 Introduction

Moisture in a wound is an important factor during the healing process. The advantages of a moist wound environment over a dry environment are several, including avoiding tissue dehydration, cell death, and the acceleration of the healing process.

However, it is important to note that there is no specific universally accepted moisture percentage value for all wounds, as moisture requirements may vary depending on the type and severity of the lesion, as well as individual patient conditions.[5][6]

For this parameter, several measurements were taken over time until the laboratory grade ultrapure Milli-Q water evaporated completely, considering t1=5 minutes, t2=15 minutes, and periodically until its total evaporation.

3.3.3.2 Bode Diagrams

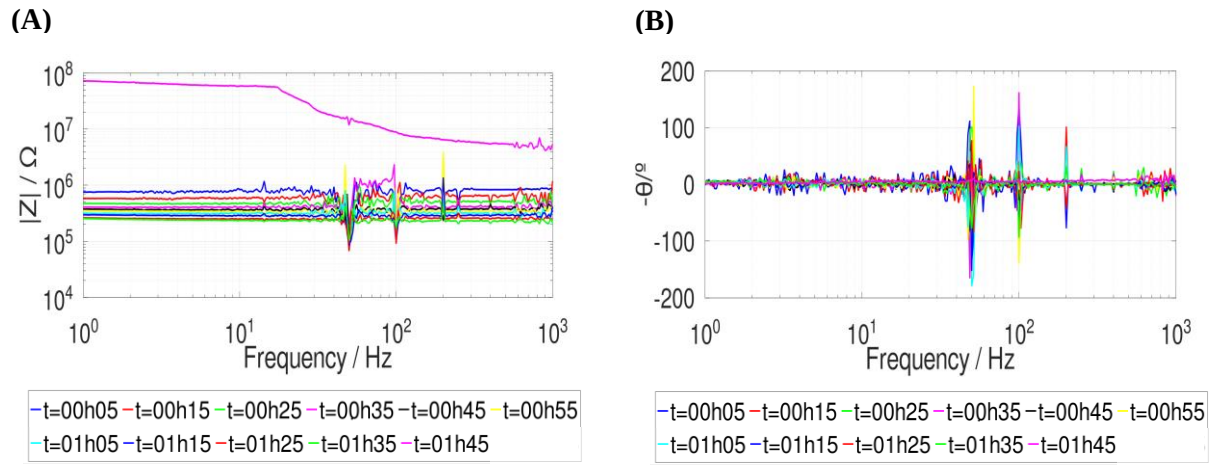

Figure 23 - Bode Diagrams for an electrode pair distance of 10 mm. A) Impedance by Frequency. (B) Phase by Frequency

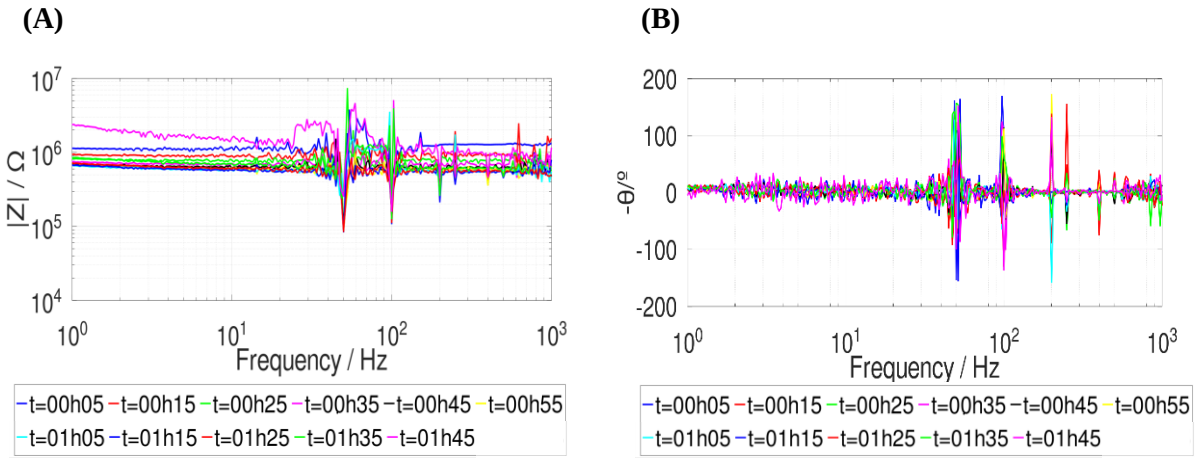

Figure 24 - Bode Diagrams for an electrode pair distance of 3 mm. A) Impedance by Frequency. (B) Phase by Frequency.

The total evaporation time for all experiments, Figure 23 and Figure 18,was 1 hours and 45 minutes. During this time, the impedance value showed a gradual decrease over time, which is explained by the decreasing concentration of H^+ ions over time that causes this change, until the electrolyte was completely evaporated, at which point, as expected, there was an abrupt increase in impedance to values of the order of 10^8. This suggests that one of the factors in wound healing was progressing positively at the time of this abrupt increase in impedance.[31]

4

CONCLUSION AND FUTURE PERSPECTIVES

4.1 Conclusion

For this application, paper was initially used as the substrate, followed by the use of an innovative water transfer technique that allowed a switch to a flexible, robust and easy-to-use substrate, polyurethane.

A detailed physico-chemical characterisation of the LIG was then carried out, which made it possible to verify that, in addition to the laser conditions of use, 5% power, 5% speed and 1000 PPI, being the most suitable for this system, the analysis of the SEM images confirmed the existence of uniform and defined LIG fibres throughout the device.A decrease in the resistive properties of the pattern, a low value of sheet resistance was reachedd, and the presence, in the Raman spectrum, of the D and G peaks characteristic of an amorphous carbon base, with an I_D/I_G ratio as low as 0.867, indicate a graphene material with few defects.

Finally, various data were collected on pH conditions and impedance values throughout the water evaporation process, in order to study the influence of humidity on the process demonstrating the success of the measurement in that, between impedance values of $9 \times 10^4\ \Omega$ and $6 \times 10^5\ \Omega$, the skin has a pH between 3.5 and 6, indicating that, at these values, the skin tissue is healthy. With regard to humidity, we can also see that between $9 \times 10^5\ \Omega$ and $1 \times 10^5\ \Omega$, the wound is still moist, i.e., the healing process is still underway.

In short, given all the considerations mentioned above, this is a system that could be used to monitor wounds in the future.

4.2 Future Perspectives

In order to significantly improve the quality of our research, it is essential to explore a number of alternatives. One of these is to extend the tests used to assess the condition of the wound to include measurements of temperature, oxygen levels in the affected area and a more precise approach to determining the exact location and size of the wound.

In addition to these considerations, it is important to try to improve the production process of the device so that it can be manufactured more uniformly and more quickly, while maintaining the expected quality.

Furthermore, we recognize the importance of moving towards in vivo testing as a crucial step in the significant development of our current system. The transition to tests on living organisms, be they animal models or, eventually, human clinical studies, will allow us to assess the effectiveness of our interventions with greater precision.

A

AN APPENDIX

A.1 Formulas Used

A.1.1 Electrical Study

$$\rho = R \times \frac{A}{L}$$
$$\sigma = \frac{1}{\rho}$$
$$R_s = R \times \frac{W}{L}$$

A.1.2 Δ Z calculate

$$\Delta Z_{3,5}(\%) = \frac{(Z_6 - Z_{3,5})}{Z_{3,5}}$$
$$\Delta Z_{4,5}(\%) = \frac{(Z_6 - Z_{4,5})}{Z_{4,5}}$$

A.2 pH variation measurements

A.2.1 Bode Diagrams - Measurements in pairs of electrodes 10 mm apart

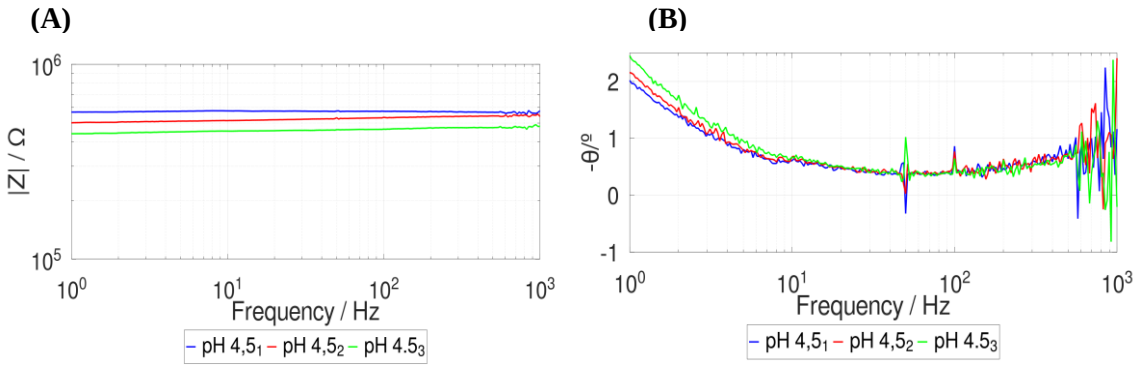

Figure 25 - Bode Diagrams at a pH of 4.5 in pairs of electrodes 10 mm apart. (A) Impedance by Frequency. (B) Phase by Frequency.

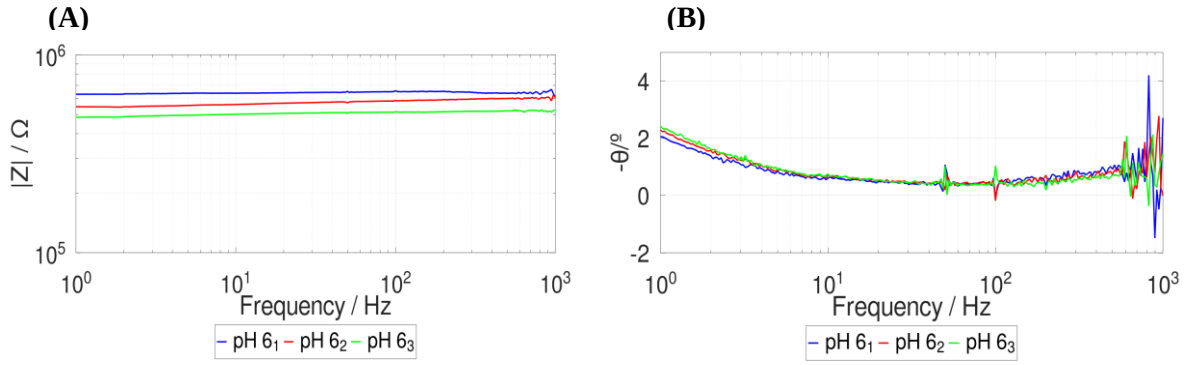

Figure 26 - Bode Diagrams at a pH of 6 in pairs of electrodes 10 mm apart. (A) Impedance by Frequency. (B) Phase by Frequency.

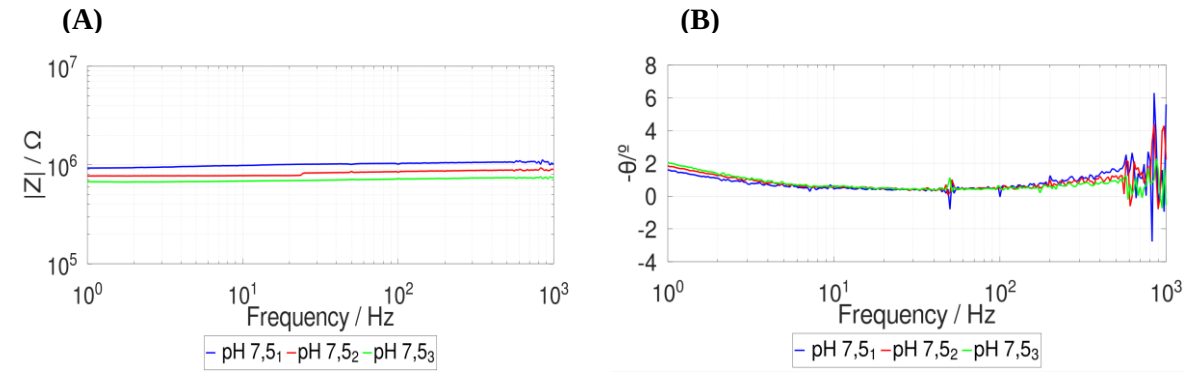

Figure 27 - Bode Diagrams at a pH of 7.5 in pairs of electrodes 10 mm apart. (A) Impedance by Frequency. (B) Phase by Frequency.

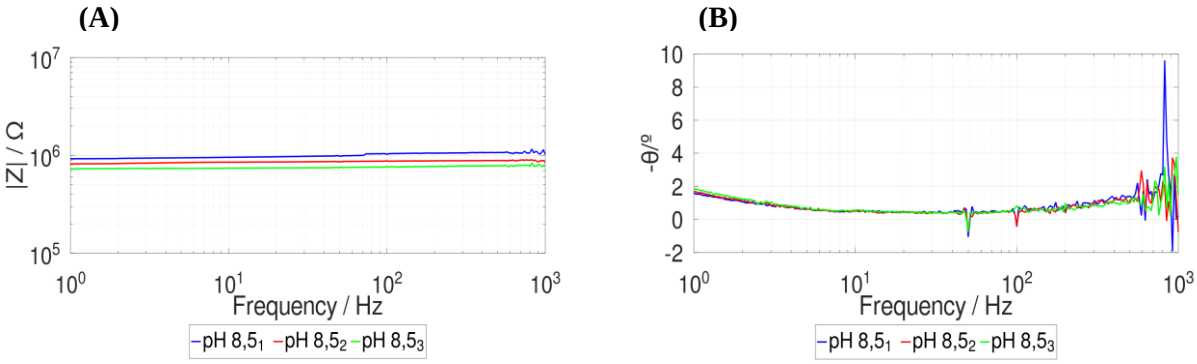

Figure 28 - Bode Diagrams at a pH of 8.5 in pairs of electrodes 10 mm apart. (A) Impedance by Frequency. (B) Phase by Frequency.

A.2.2 Bode Diagrams - Measurements in pairs of electrodes 3 mm apart

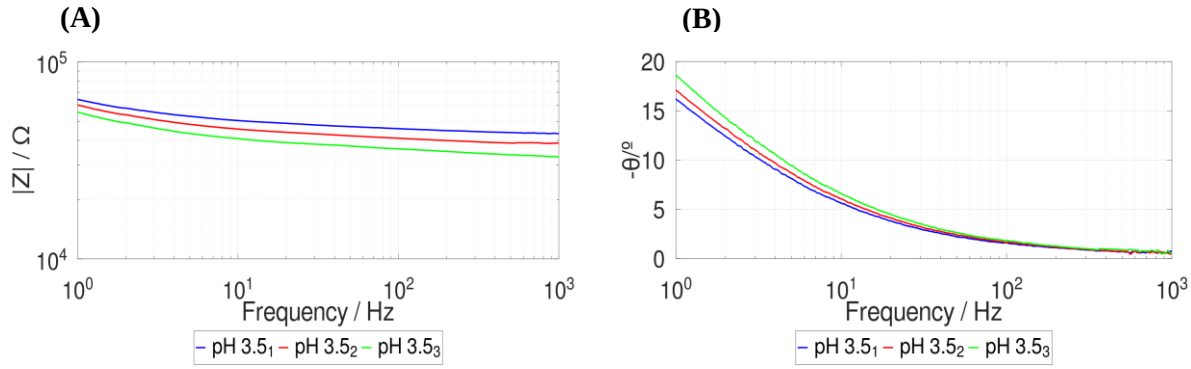

Figure 29 - Bode Diagrams at a pH of 3.5 in pairs of electrodes 3 mm apart. (A) Impedance by Frequency. (B) Phase by Frequency.

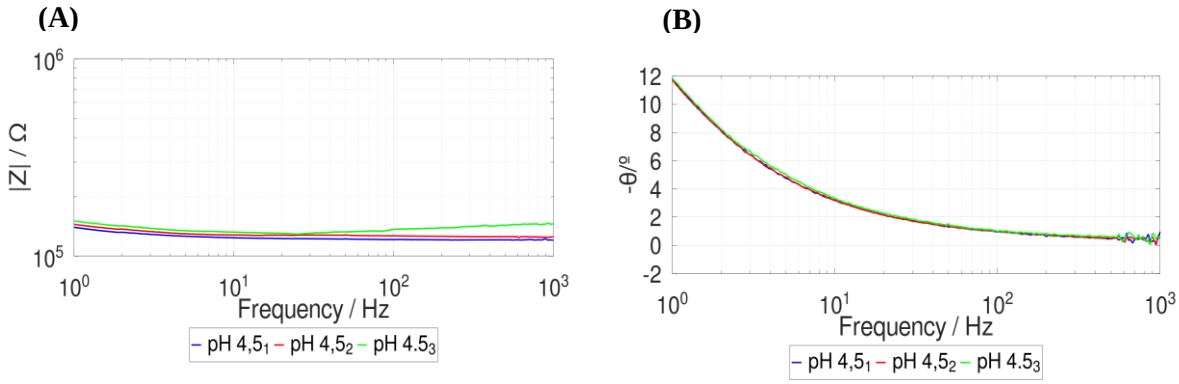

Figure 30 - Bode Diagrams at a pH of 4.5 in pairs of electrodes 3 mm apart. (A) Impedance by Frequency. (B) Phase by Frequency.

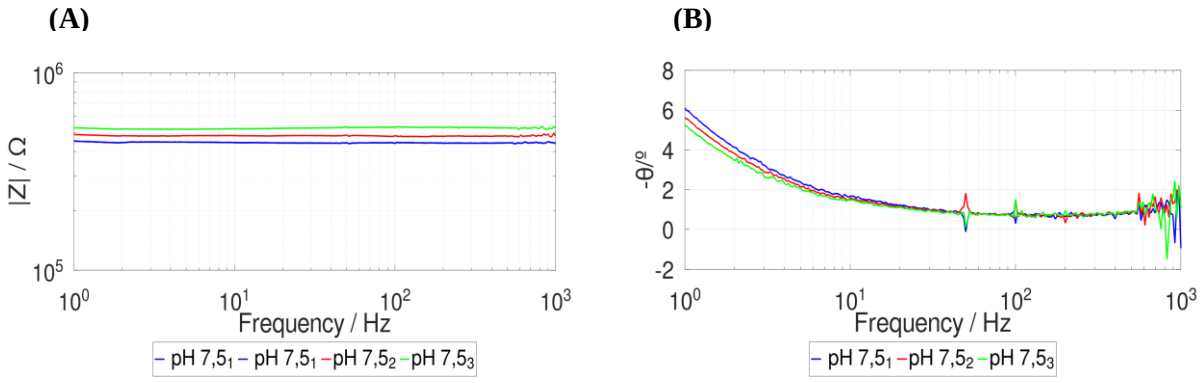

Figure 31 - Bode Diagrams at a pH of 7.5 in pairs of electrodes 3 mm apart. (A) Impedance by Frequency. (B) Phase by Frequency.

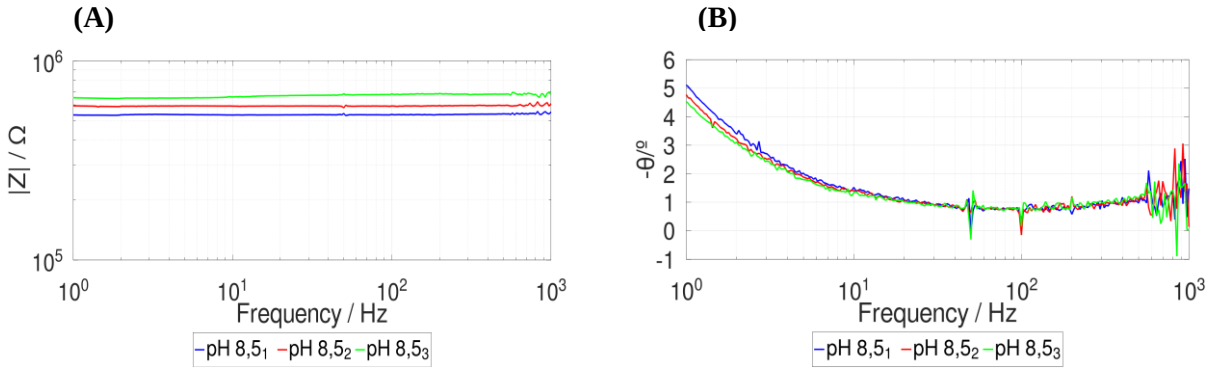

Figure 32 - Bode Diagrams at a pH of 8.5 in pairs of electrodes 3 mm apart. (A) Impedance by Frequency. (B) Phase by Frequency.

A.2.3 Bode Diagrams - Differences between Distance

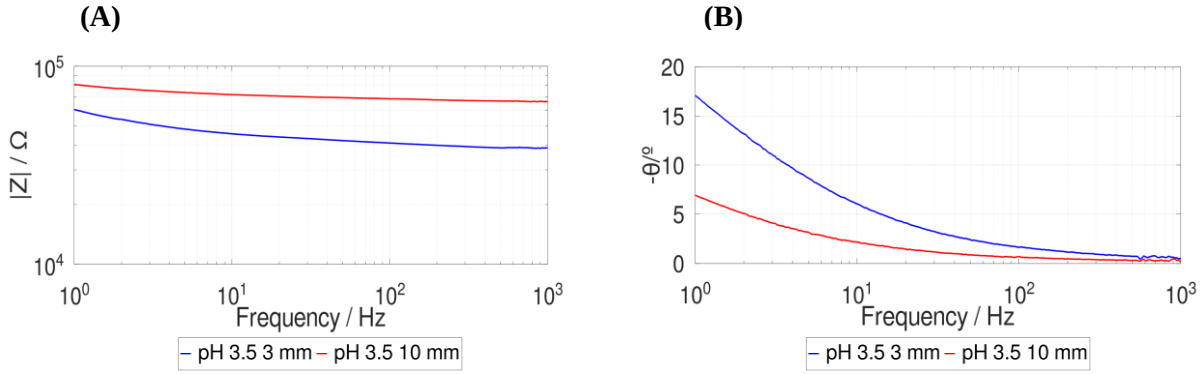

Figure 33 - Bode Diagrams at a pH of 3.5 in pairs of electrodes 3 mm and 10 mm apart. (A) Impedance by Frequency. (B) Phase by Frequency.

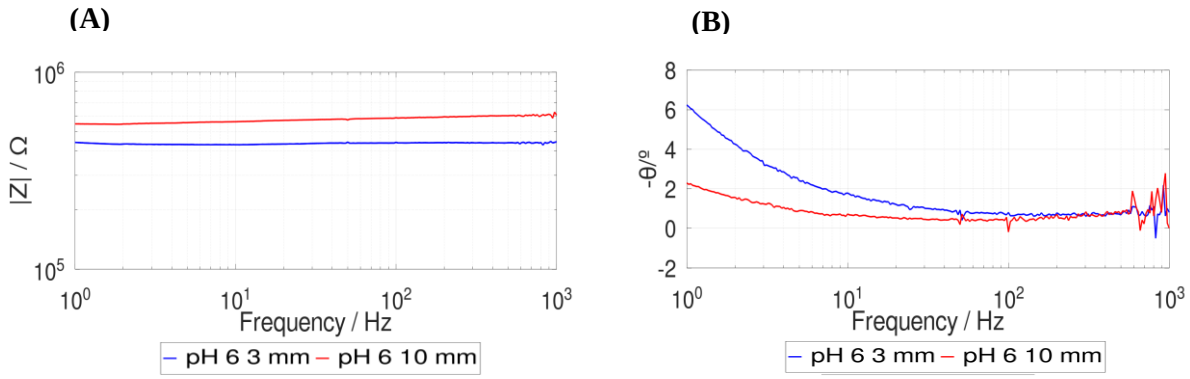

Figure 34 - Bode Diagrams at a pH of 6 in pairs of electrodes 3 mm and 10 mm apart. (A) Impedance by Frequency. (B) Phase by Frequency.

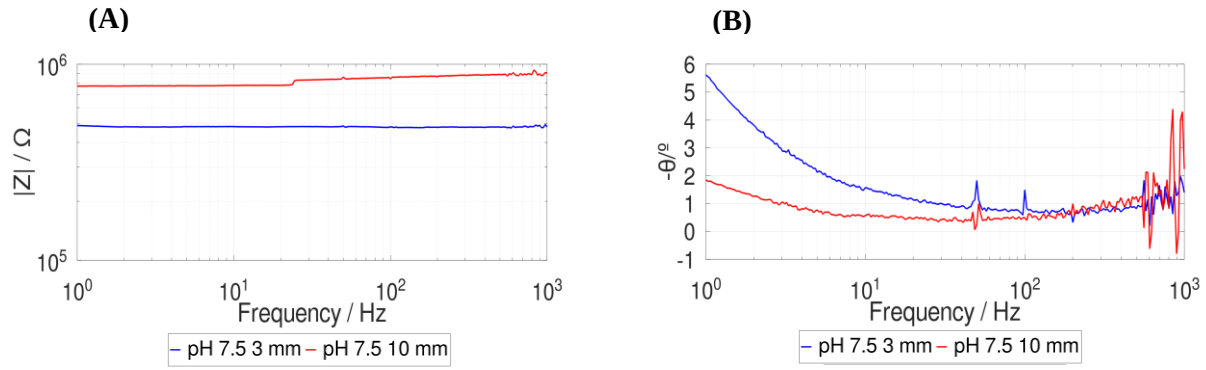

Figure 35 - Bode Diagrams at a pH of 7.5 in pairs of electrodes 3 mm and 10 mm apart. (A) Impedance by Frequency. (B) Phase by Frequency.

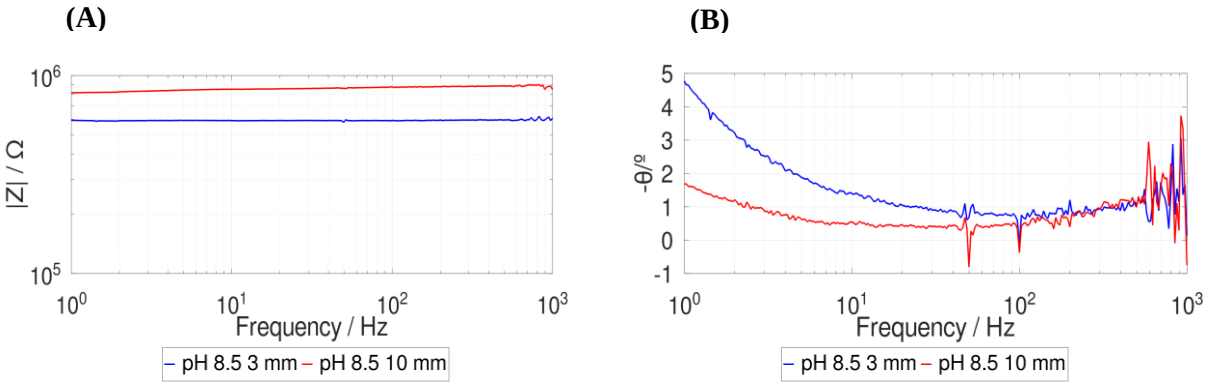

Figure 36 - Bode Diagrams at a pH of 8.5 in pairs of electrodes 3 mm and 10 mm apart. (A) Impedance by Frequency. (B) Phase by Frequency.

Bibliography

[1] S. L. Swisher *et al.*, "Impedance sensing device enables early detection of pressure ulcers in vivo," *Nat. Commun.*, vol. 6, no. 1, p. 6575, May 2015, doi: 10.1038/ncomms7575.

[2] M. Ochoa, R. Rahimi, and B. Ziaie, "Flexible Sensors for Chronic Wound Management," *IEEE Rev. Biomed. Eng.*, vol. 7, pp. 73–86, 2014, doi: 10.1109/RBME.2013.2295817.

[3] E. Heuss, *Die Reaktion des schweisses beim gesunden menschen*. Voss, 1892.

[4] H. Schade and A. Marchionini, "Der säuremantel der haut (nach gaskettenmessungen)," *Klin. Wochenschr.*, vol. 7, no. 1, pp. 12–14, 1928.

[5] C. K. Field and M. D. Kerstein, "Overview of wound healing in a moist environment," *Am. J. Surg.*, vol. 167, no. 1, Supplement, pp. S2–S6, 1994, doi: https://doi.org/10.1016/0002-9610(94)90002-7.

[6] P.-G. Su, W.-C. Li, J.-Y. Tseng, and C.-J. Ho, "Fully transparent and flexible humidity sensors fabricated by layer-by-layer self-assembly of thin film of poly(2-acrylamido-2-methylpropane sulfonate) and its salt complex," *Sensors Actuators B Chem.*, vol. 153, no. 1, pp. 29–36, Mar. 2011, doi: 10.1016/j.snb.2010.09.074.

[7] A. Kekonen *et al.*, "Bioimpedance method for monitoring venous ulcers: Clinical proof-of-concept study," *Biosens. Bioelectron.*, vol. 178, no. December 2020, p. 112974, Apr. 2021, doi: 10.1016/j.bios.2021.112974.

[8] M.-J. Chaudon, O. Hulea, A. Yakoub, P. Monnier, and M. Saadaoui, "Wearable device for iontophoretic treatment and monitoring of pressure ulcers: Proof-of-concept," *Med. Eng. Phys.*, vol. 107, no. July, p. 103861, Sep. 2022, doi: 10.1016/j.medengphy.2022.103861.

[9] J. Mudondo *et al.*, "Recent Advances in the Chemobiological Upcycling of Polyethylene Terephthalate (PET) into Value-Added Chemicals," *J. Microbiol. Biotechnol.*, vol. 33, no. 1, pp. 1–14, Jan. 2023, doi: 10.4014/jmb.2208.08048.

[10] A. Das and P. Mahanwar, "A brief discussion on advances in polyurethane applications," *Adv. Ind. Eng. Polym. Res.*, vol. 3, no. 3, pp. 93–101, 2020, doi: 10.1016/j.aiepr.2020.07.002.

[11] J. S. Stefano *et al.*, "Different approaches for fabrication of low-cost electrochemical sensors," *Curr. Opin. Electrochem.*, vol. 32, p. 100893, Apr. 2022, doi: 10.1016/j.coelec.2021.100893.

[12] L. Torrisi, L. Silipigni, and M. Cutroneo, "Radiation effects of IR laser on graphene oxide irradiated in vacuum and in air," *Vacuum*, vol. 153, pp. 122–131, Jul. 2018, doi: 10.1016/j.vacuum.2018.04.010.

[13] R. Ye, D. K. James, and J. M. Tour, "Laser-Induced Graphene," *Acc. Chem. Res.*, vol. 51, no. 7, pp. 1609–1620, Jul. 2018, doi: 10.1021/acs.accounts.8b00084.

[14] J. Lin *et al.*, "Laser-induced porous graphene films from commercial polymers," *Nat. Commun.*, vol. 5, no. 1, p. 5714, Dec. 2014, doi: 10.1038/ncomms6714.

[15] L. Huang, J. Su, Y. Song, and R. Ye, "Laser-Induced Graphene: En Route to Smart Sensing," *Nano-Micro Lett.*, vol. 12, no. 1, p. 157, Dec. 2020, doi: 10.1007/s40820-020-00496-0.

[16] A. C. Lazanas and M. I. Prodromidis, "Electrochemical Impedance Spectroscopy—A Tutorial," *ACS Meas. Sci. Au*, vol. 3, no. 3, pp. 162–193, Jun. 2023, doi:

10.1021/acsmeasuresciau.2c00070.
[17] C. M. A. Brett, "Electrochemical Impedance Spectroscopy in the Characterisation and Application of Modified Electrodes for Electrochemical Sensors and Biosensors," *Molecules*, vol. 27, no. 5, 2022, doi: 10.3390/molecules27051497.
[18] T. Pinheiro *et al.*, "Water Peel-Off Transfer of Electronically Enhanced, Paper-Based Laser-Induced Graphene for Wearable Electronics," *ACS Nano*, vol. 16, no. 12, pp. 20633–20646, Dec. 2022, doi: 10.1021/acsnano.2c07596.
[19] T. Pinheiro *et al.*, "Influence of CO 2 laser beam modelling on electronic and electrochemical properties of paper-based laser-induced graphene for disposable pH electrochemical sensors," vol. 11, no. May, 2023, doi: 10.1016/j.cartre.2023.100271.
[20] J. Coelho *et al.*, "Paper-based laser-induced graphene for sustainable and flexible microsupercapacitor applications," *Microchim. Acta*, vol. 190, no. 1, p. 40, Jan. 2023, doi: 10.1007/s00604-022-05610-0.
[21] H. Liu *et al.*, "Laser-induced and KOH-activated 3D graphene: A flexible activated electrode fabricated via direct laser writing for in-plane micro-supercapacitors," *Chem. Eng. J.*, vol. 393, p. 124672, 2020, doi: https://doi.org/10.1016/j.cej.2020.124672.
[22] M. G. Stanford, K. Yang, Y. Chyan, C. Kittrell, and J. M. Tour, "Laser-Induced Graphene for Flexible and Embeddable Gas Sensors," *ACS Nano*, vol. 13, no. 3, pp. 3474–3482, 2019, doi: 10.1021/acsnano.8b09622.
[23] Y. Chyan, J. Cohen, W. Wang, C. Zhang, and J. M. Tour, "Graphene Art," *ACS Appl. Nano Mater.*, vol. 2, no. 5, pp. 3007–3011, 2019, doi: 10.1021/acsanm.9b00391.
[24] B. Kulyk *et al.*, "Laser-Induced Graphene from Paper for Mechanical Sensing," *ACS Appl. Mater. \& Interfaces*, vol. 13, no. 8, pp. 10210–10221, 2021, doi: 10.1021/acsami.0c20270.
[25] J. Wu, M. Lin, X. Cong, H. Liu, P. Tan, and M. Lin, "Chem Soc Rev and its applications in related devices," pp. 1822–1873, 2018, doi: 10.1039/c6cs00915h.
[26] T. Guinovart, G. Valdés-Ramírez, J. R. Windmiller, F. J. Andrade, and J. Wang, "Bandage-Based Wearable Potentiometric Sensor for Monitoring Wound pH," *Electroanalysis*, vol. 26, no. 6, pp. 1345–1353, Jun. 2014, doi: 10.1002/elan.201300558.
[27] L. A. Schneider, A. Korber, S. Grabbe, and J. Dissemond, "Influence of pH on wound-healing: A new perspective for wound-therapy?," *Arch. Dermatol. Res.*, vol. 298, no. 9, pp. 413–420, 2007, doi: 10.1007/s00403-006-0713-x.
[28] L. Manjakkal, E. Djurdjic, K. Cvejin, J. Kulawik, K. Zaraska, and D. Szwagierczak, "Electrochemical Impedance Spectroscopic Analysis of RuO2 Based Thick Film pH Sensors," *Electrochim. Acta*, vol. 168, pp. 246–255, 2015, doi: https://doi.org/10.1016/j.electacta.2015.04.048.
[29] C. A. Shiffman, "Adverse effects of near current-electrode placement in non-invasive bio-impedance measurements," *Physiol. Meas.*, vol. 34, no. 11, p. 1513, 2013, doi: 10.1088/0967-3334/34/11/1513.
[30] J. Alvarez-Ramirez, J. Vazquez-Arenas, M. González, and Y. Carrera-Tarela, "Non-Linear First-Harmonic Balance to Compute the Electrochemical Impedance of Butler-Volmer Equation," *J. Electrochem. Soc.*, vol. 165, no. 9, pp. H517–H523, 2018, doi: 10.1149/2.1091809jes.
[31] S. Agarwal and G. L. Sharma, "Humidity sensing properties of (Ba, Sr) TiO3 thin films grown by hydrothermal–electrochemical method," *Sensors Actuators B Chem.*, vol. 85, no. 3, pp. 205–211, 2002, doi: https://doi.org/10.1016/S0925-4005(02)00109-0.